Decrease of electrical resistivity in $Ca_3Co_4O_9$ thermoelectric ceramics by Ti doping

M. A. Torres[1], Sh. Rasekh[1], P. Bosque[2], G. Constantinescu[1], M. A. Madre[1], J. C. Diez[1], A. Sotelo[1]

[1]ICMA (Universidad de Zaragoza-CSIC), C/María de Luna 3, E-50018, Zaragoza (Spain)

[2]Centro Universitario de la Defensa de Zaragoza. Academia General Militar. Ctra. de Huesca s/n. 50090-Zaragoza (Spain).

Abstract

$Ca_3Co_{4-x}Ti_xO_9$ polycrystalline thermoelectric ceramics with small amounts of Ti have been prepared by the classical solid state method. X-ray diffraction data have shown that $Ca_3Co_4O_9$ is the major phase, with small amounts of the $Ca_3Co_2O_6$ one. Moreover, they show that Ti has been incorporated into these two phases. Electrical resistivity decreases, compared with the values for undoped samples, until 0.03-Ti doped ones. Further Ti addition produces an increase of resistivity with respect to the 0.03 Ti doped samples. Seebeck coefficient does not appreciably change in all the measured temperature range, independently of Ti content. The improvement in electrical resistivity leads about 55 % higher power factor values for the 0.03 Ti-doped samples than the obtained in the undoped ones. The maximum power factor at 800 ºC, around 0.33 $mW/K^2.m$, is slightly higher than the obtained in higher density samples,

clearly indicating the good thermoelectric performances of these doped samples.

Keywords: Ceramics; Cobalt oxides; Electrical resistivity; Seebeck coefficient.

Corresponding author: M. A. Madre

e-mail: amadre@unizar.es

Address: ICMA (CSIC-Universidad de Zaragoza) C/Mª de Luna, 3; 50018-Zaragoza; Spain

Tel: +34 976762617

Fax: +34 976761958

1. Introduction

Thermoelectric (TE) materials are gaining interest due to their ability to directly transform a temperature difference to electrical power. As a consequence, this technology is regarded as one of the most promising methods to harvest energy from wasted and/or natural heat sources. As examples, some of the target practical applications for these materials are, for example, in waste heat recovery devices [1], solar thermoelectric generators [2], or cooling devices [3]. On the other hand, it is necessary to obtain high energy conversion materials in order to be considered for practical applications. The efficiency of these materials is usually quantified by the figure of merit ($ZT=TS^2/\rho\kappa$), where S, ρ, κ, and T are the Seebeck coefficient, electrical resistivity, thermal conductivity, and the absolute temperature, respectively [4]. In ZT expression, the electrical part (S^2/ρ) is called power factor, PF, which is often used to characterise the performances of TE materials.

Nowadays, intermetallic materials-based devices can be found in some practical applications, as energy harvesters in vehicles exhaust. However, these kind of materials can suffer degradation and/or oxidation when working under air at high temperatures. Other important environmental problem is that they are often composed of heavy and/or toxic elements, as Te, Sb, etc. All these temperature limitations were surpassed by the discovery of high thermoelectric properties in the Na-Co-O system [5]. Since then, many works have been carried out on the cobalt-based ceramics for high temperature applications, mainly on the $Ca_3Co_4O_9$ [6,7] $Bi_2Sr_2Co_2O_x$ [8,9], $Bi_2Ca_2Co_2O_x$ [10,11] and $Bi_2Ba_2Co_2O_x$ [12,13] systems. All of them are characterized by high thermoelectric properties and working temperatures.

The studies on single crystals of these materials have demonstrated that they can be described using a monoclinic structure which is composed of two different layers. These layers form an alternate stacking of a common conductive CdI_2-type hexagonal CoO_2 layer with a two-dimensional triangular lattice and a block layer composed of insulating rock-salt-type (RS) layers. The two sublattices (RS block and CdI_2-type CoO_2 layer) are characterized by common a- and c-axis lattice parameters and β angles, but different b-axis length, leading to a misfit along the b-direction [14]. This high structural anisotropy is reflected in the formation of plate-like grains during the crystallisation process. In these grains, the preferential growth plane is coinciding with the conducting one, fact which can be exploited to texture the bulk materials by different methods. Such processes allow the alignment of the conducting planes in polycrystalline samples leading to macroscopic properties comparable to those obtained on single crystals. Many methods have been reported to be efficient to produce well aligned bulk materials, in these or in similar anisotropic systems, such as hot uniaxial pressing [15], spark plasma sintering [16], laser floating zone melting (LFZ) [17], electrically assisted laser floating zone [18], *etc*. The main drawbacks of these methods are due to different factors, as the relatively long treatments, the high costs associated with the processes and/or the strong dependence on the growth or the texturing speed [15,16,19,20].

It has also been reported that the Seebeck coefficient and electrical resistivity values are governed by the incommensurability ratio and/or the charge of the RS block layer between the CoO_2 ones [21] which provides the basis for the modification of thermoelectric properties by doping. The most common ones are

based on the substitution of an alkaline-earth [22,23], Co [24,25], or Bi [26,27] which have demonstrated their suitability for improving the materials performances.

The aim of this work is studying the effect of Ti substitution for Co in $Ca_3Co_{4-x}Ti_xO_9$ TE ceramic materials prepared by the solid state route. The modification of microstructural and high temperature thermoelectric properties has been determined as a function of Ti content.

2. Experimental

The $Ca_3Co_{4-x}Ti_xO_9$ polycrystalline ceramic materials, with x = 0.00, 0.01, 0.03, 0.05, and 0.07, used in this work were prepared by the conventional solid state route from commercial $CaCO_3$ (Panreac, 98 + %), Co_2O_3 (Aldrich, 98 + %), and TiO_2 (Aldrich, $\geq$ 99 %) powders as starting materials. They were weighed in the adequate proportions, mixed and ball milled in an agate ball mill for 30 minutes, at 300 rpm, in acetone media. The suspension has been heated under infrared radiation until all the acetone has been evaporated. The dry mixture was then manually milled and thermally treated twice at 750 and 800 ºC for 12h under air, with an intermediate manual grinding to assure the total $CaCO_3$ decomposition as reported in previous works [28]. After the thermal treatments, the powders were uniaxially pressed at 400 MPa in form of parallelepipeds (~ 3 mm x 3 mm x 14 mm) and sintered at 910 ºC for 24 h with a final furnace cooling.

Powder X-ray diffraction (XRD) patterns have been used to identify the different phases in the sintered materials. Data have been collected at room temperature, with 2θ ranging between 5 and 60 degrees, using a Rigaku

D/max-B X-ray powder diffractometer working with Cu Kα radiation using a graphite monochromator.

Microstructural observations were performed on longitudinal sections and fractured surfaced of the samples, using a Field Emission Scanning Electron Microscope (FESEM, Carl Zeiss Merlin) equipped with an energy dispersive X-ray spectrometer (EDX). Micrographs of the surfaces have been used to analyze the different phases and their distribution. Apparent density measurements have been performed on several samples for each composition after sintering, using 4.677 g/cm^3 as theoretical density [29]. Oxygen content was determined in some of the annealed materials by cerimetric titrations, as described elsewhere [7].

Electrical resistivity and Seebeck coefficient were simultaneously determined by the standard dc four-probe technique in a LSR-3 measurement system (Linseis GmbH), in the steady state mode and at temperatures between 50 and 800 ºC under He atmosphere. Moreover, with the electrical resistivity and thermopower data, PF has been calculated to determine the samples performances. These properties have been compared with the results obtained in the undoped samples and with those reported in the literature.

3. Results and discussion

Powder XRD patterns for the different $Ca_3Co_{4-x}Ti_xO_9$ samples are displayed in Fig. 1 (from 5 to 40º for clarity). In the plot it can be clearly seen that all the samples have similar diffraction patterns and that the major phase is the thermoelectric $Ca_3Co_{4-x}Ti_xO_9$ one. As can be observed for the undoped samples (Fig. 1a), the highest peaks have been associated to the thermoelectric

$Ca_3Co_4O_9$ phase, indicated by its reflection planes, in agreement with previously reported data [30], where a monoclinic unit cell (#12, C12/m1) has been used. On the other hand, the peaks identified by * in Fig. 1a correspond to the $Ca_3Co_2O_6$ phase, in agreement with published data [31], with a rhombohedral unit cell (#167, $R\bar{3}cH$). Careful observation of these patterns shows that the $Ca_3Co_2O_6$ secondary phase content is slightly decreased when the Ti amount is raised, as can be deduced from the lower intensity of its diffraction peaks. This trend has been confirmed by the increase in the relationship between the intensities of the $Ca_3Co_4O_9$ (002) diffraction peak and the $Ca_3Co_2O_6$ (110) one. Moreover, no Ti-based secondary phases have been detected with this technique, indicating that Ti has been incorporated in the $Ca_3Co_4O_9$ and/or $Ca_3Co_2O_6$ crystal structures.

General SEM observations performed on representative fractured sections of the samples are shown in Fig. 2. In the micrographs, it can be observed that both samples possess very similar microstructure. They are formed by randomly oriented plate-like grains, which is the typical microstructure for solid state sintered samples. Moreover, it is evident that grain sizes are not homogeneous all along the samples. This effect reflects the well-known drawbacks of the classical solid state synthesis methods. On the other hand, it can be seen that the grain sizes increase with the Ti doping. Other feature observed in these micrographs is the porosity observed in the figure which seems to be similar in all cases. In order to confirm this observation, apparent density measurements have been performed in all samples. For each composition, at least three samples were used to determine their densities. Moreover, each sample was measured for three times to minimize

measurement errors. The obtained results showed that all samples possess very similar densities, ranging from about 74 % of the theoretical one for the undoped samples to ~ 76 % for the Ti-doped ones. These relatively low densities can be easily explained due to the fact that the sintering temperature used in this work (910 ºC) is far from the melting temperature of this system (~ 1350 ºC), leading to very slow densification kinetics [32]. On the other hand, the sintering temperature is very close to the maximum stability one for the $Ca_3Co_4O_9$ phase (about 925 ºC) [32].

When observing the samples surfaces shown in Fig. 3 for the undoped and 0.03 Ti doped samples, they show roughly the same plate-like grains as observed previously. Moreover, two different phases can be observed in the micrographs, the grey plate-like grains (identified by EDX as $Ca_3Co_{4-x}Ti_xO_9$), and a very similar contrast grains with different shape (indicated by arrows in the pictures) corresponding to the $Ca_3Co_{2-x}Ti_xO_6$ secondary phase. In a first sight, it is evident that the sizes and amount of this last phase are decreasing when the Ti substitution is increased, in agreement with the XRD data previously discussed. EDX analysis of the different phases has shown that Ti substitutes Co in the $Ca_3Co_4O_9$ and $Ca_3Co_2O_6$ phase in, approximately, the nominal proportion, confirming the incorporation of Ti in these crystal structures.

Fig. 4 shows the variation of the Seebeck coefficient with the temperature, as a function of the Ti doping. In the plot, it can be clearly seen that the sign of the thermopower is positive for the entire measured temperature range, which confirms a conduction mechanism mainly governed by holes. The values of the Seebeck coefficient increase with the temperature, with very similar values and behaviour for all the samples. The similar values obtained for all samples

indicate that small Ti addition does not affect, in a great extent, the $Ca_3Co_4O_9$ conduction band [33]. The obtained values at room temperature and 800 ºC (~ 135 and ~ 215 μV/K, respectively) are slightly higher than those reported elsewhere for pure and 0.1 Ti doped samples prepared under high pressure and sintered under O_2 atmosphere (~ 125 and 200-210 μV/K at the same temperatures) [34]. Moreover, the maximum Seebeck coefficient value (~ 215 μV/K) obtained in this work at 800 ºC is significantly higher than the values obtained for $Ca_3Co_4O_9$ samples prepared by autocombustion method and consolidated by spark plasma sintering (150 and 165 μV/K measured parallel and perpendicular to the applied load, respectively) at the same temperature [35].

The absolute oxygen content was determined on sintered samples by cerimetric analysis. For each substitution four determinations were performed, showing a reproducibility of around ± 0.008 for each sample. The obtained mean values are approximately the same and correspond to mean Co valences of ~ 3.16. These results agree with the measured room temperature Seebeck values which are roughly the same for all the samples.

In spite of the absence of modifications in the Seebeck coefficient by Ti doping, the electrical resistivity is clearly decreasing. This effect can be observed in Fig. 5 where the temperature dependence of electrical resistivity, as a function of the Ti content, is shown. The curve corresponding to the undoped samples shows a semiconducting-like ($d\rho/dT < 0$) behaviour, from room temperature to around 400 ºC, in agreement with previously reported data in this system where the charge transport process is a hole hopping from Co^{4+} to Co^{3+} [36]. At higher temperatures, this behaviour changes to a metallic-like one ($d\rho/dT > 0$) where

the charge carriers are transported in the valence or conduction band [25]. Ti addition modifies the resistivity behaviour with temperature which is nearly metallic-like for Ti contents > 0.01. In these doped samples, room temperature resistivity values decrease until 0.03 Ti content and then increase for further Ti addition. The lowest measured room temperature resistivity values (~ 12.5 mΩ.cm for the 0.03 Ti-substituted samples) are slower than those reported elsewhere for 0.1 Ti doped samples prepared under high pressure and sintered under O_2 atmosphere (~ 18 mΩ.cm at the same temperature) [34]. Taking into account these data, the results obtained in this work are more impressive, as annealing under O_2 atmosphere should raise the Co^{4+} content which, in turn, should increase the carrier concentration and, as a consequence, decrease the electrical resistivity of these samples.

In order to evaluate the thermoelectric performances of these materials, the power factor has been calculated using the electrical resistivity and Seebeck coefficient data and plotted as a function of temperature in Fig. 6. When considering PF values at about 50 ºC (~ room temperature), it can be clearly seen that the Ti-doped samples possess higher PF values than the undoped ones (between 30 to 60 %). The highest PF value obtained at 800 ºC (around 0.33 mW/K^2.m) for the 0.03 Ti-doped samples is ~ 55 % higher than the obtained for the undoped samples. This maximum PF value is slightly higher than the obtained in samples with 0.1 Ti substitution prepared under high pressures (~ 0.31 mW/K^2.m) [34]. In any case, the values obtained in this work are more impressive if it is taken into account that these values reported in the literature have been obtained in samples prepared by methods which should produce much higher density materials.

All these data indicate that small Ti additions can improve significantly the thermoelectric performances of $Ca_3Co_4O_9$ ceramics, when a simple but careful solid state preparation route, is employed thus approaching them to their commercial and practical applications.

4. Conclusions

This paper demonstrates that small Ti substitutions for Co in $Ca_3Co_4O_9$ samples are useful to improve its thermoelectric performances. This improvement is due to a decrease on the electrical resistivity of samples without appreciably modifying the Seebeck coefficient values. The optimal Ti for Co substitution has been determined with respect to the power factor values at 50 and 800 ºC, which is maximum for the 0.03 Ti-doped samples. The raise in PF, compared with the undoped samples, is around 55 % at both temperatures, with values about 0.15 and 0.33 $mW/K^2.m$, at 50 and 800 ºC, respectively. Moreover, the measured PF values at 800 ºC are around the best ones reported in the literature on higher density materials.

Acknowledgements

The authors wish to thank the MINECO-FEDER (Project MAT2013-46505-C3-1-R) and the Gobierno de Aragón (Research Groups T12 and T87) for financial support. Authors would also like to acknowledge the use of Servicio General de Apoyo a la Investigación-SAI, Universidad de Zaragoza. The technical contributions of C. Estepa, and C. Gallego are also acknowledged.

References

1. G. Mahan, B. Sales, J. Sharp, Phys. Today 50, 42 (1997)

2. H. Naito, Y. Kohsaka, D. Cooke, H. Arashi, Solar Energy 58, 191 (1996)

3. M. H. Elsheikh, D. A. Shnawah, M. F. M. Sabri, S. B. M. Said, M. H. Hassan, M. B. A. Bashir, M. Mohamad, Renew. Sust. Energ. Rev. 30, 337 (2014)

4. D. M. Rowe, in Thermoelectrics handbook: macro to nano, ed By D. M. Rowe (CRC Press, Boca Raton, FL, 2006) p. 1-3

5. I. Terasaki, Y. Sasago, K. Uchinokura, Phys. Rev. B 56, 12685 (1997)

6. Y. Huang, B. Zhao, J. Fang, R. Ang, Y. Sun, J. Appl. Phys. 110, 123713 (2011)

7. A. Sotelo, G. Constantinescu, Sh. Rasekh, M. A. Torres, J. C. Diez, M. A. Madre, J. Eur. Ceram. Soc. 32, 2415 (2012)

8. N. Sun, S. T. Dong, B. B. Zhang, Y. B. Chen, J. Zhou, S. T. Zhang, Z. B. Gu, S. H. Yao, Y. F. Chen, J. Appl. Phys. 114, 043705 (2013)

9. J. C. Diez, E. Guilmeau, M. A. Madre, S. Marinel, S. Lemmonier, A. Sotelo, Solid State Ionics 180, 827 (2009)

10. X. G. Luo, Y. C. Jing, H. Chen, X. H. Chen, J. Crystal Growth 308, 309 (2007)

11. A. Sotelo, E. Guilmeau, Sh. Rasekh, M. A. Madre, S. Marinel, J. C. Diez, J. Eur. Ceram. Soc. 30, 1815 (2010)

12. R. Ang, Y. P. Sun, X. Luo, W. H. Song, J. Appl. Phys. 102, 073721 (2007)

13. Sh. Rasekh, G. Constantinescu, M. A. Torres, M. A. Madre, J. C. Diez, A. Sotelo, Adv. Appl. Ceram. 111, 490 (2012)

14. Y. Miyazaki, Solid State Ionics 172, 463 (2004)

15. H. Wang, X. Sun, X. Yan, D. Huo, X. Li, J.-G. Li, X. Ding, J. Alloys Compds. 582, 294 (2014)

16. S. Butt, Y.-C- Liu, J.-L. Lan, K. Shehzad, B. Zhan, Y. Lin, C.-W. Nan, J. Alloys Compds. 588, 277 (2014)

17. A. Sotelo, E. Guilmeau, M. A. Madre, S. Marinel, S. Lemmonier, J. C. Diez, Bol. Soc. Esp. Ceram. V. 47, 225 (2008)

18. N. M. Ferreira, Sh. Rasekh, F. M. Costa, M. A. Madre, A. Sotelo, J.C. Diez, M. A. Torres, Mater. Lett. 83, 144 (2012)

19. J. C. Diez, Sh. Rasekh, M. A. Madre, E. Guilmeau, S. Marinel, A. Sotelo, J. Electron. Mater. 39, 1601 (2010)

20. G. Constantinescu, Sh. Rasekh, M. A. Torres, M. A. Madre, J. C. Diez, A. Sotelo, Scripta Mater. 68, 75 (2013)

21. A. Maignan, D. Pelloquin, S. Hébert, Y. Klein, M. Hervieu, Bol. Soc. Esp. Ceram. V. 45, 122 (2006)

22. G. Constantinescu, Sh. Rasekh, M. A. Torres, J. C. Diez, M. A. Madre, A. Sotelo, J. Alloys Compds. 577, 511 (2013)

23. S. Demirel, M. A. Aksan, S. Altin, J. Mater. Sci.: Mater. Electron. 23, 2251 (2012)

24. J. C. Diez, M. A. Torres, Sh. Rasekh, G. Constantinescu, M. A. Madre, A. Sotelo, Ceram. Int. 39, 6051 (2013)

25. S. Pinitsoontorn, N. Lerssongkram, N. Keawprak, V. Amornkitbamrung, J. Mater. Sci.: Mater. Electron. 23, 1050 (2012)

26. A. Sotelo, Sh. Rasekh, E. Guilmeau, M. A. Madre, M. A. Torres, S. Marinel, J. C. Diez, Mater. Res. Bull. 46, 2537 (2011)

27. J. Liu, H. S. Yang, Y. S. Chai, L. Zhu, H. Qu, C. H. Sun, H. X. Gao, X. D. Chen, K. Q. Ruan, L. Z. Cao, Phys. Lett. A 356, 85 (2006)

28. G. Constantinescu, M. A. Torres, Sh. Rasekh, M. A. Madre, J. C. Diez, A. Sotelo, J. Mater. Sci.: Mater. Electron. 25, 922 (2014)

29. M. A. Madre, F. M. Costa, N. M. Ferreira, A. Sotelo, M. A. Torres, G. Constantinescu, Sh. Rasekh, J. C. Diez, J. Eur. Ceram. Soc. 33, 1747 (2013)

30. T. Kajitani, K. Yubuta, X. Y. Huang, Y. Miyazaki, J. Electron. Mater. 38, 1462 (2009)

31. C. H. Hervoches, H. Okamoto, A. Kjekshus, H. Fjellvag, B. Hauback, J. Solid State Chem. 182, 331 (2009)

32. D. Sedmidubský, V. Jakes, O. Jankovský, J. Leitner, Z. Sofer, J. Hejtmánek, J. Solid State Chem. 194, 199 (2012)

33. Sh. Rasekh, M. A. Torres, G. Constantinescu, M. A. Madre, J. C. Diez, A. Sotelo, J. Mater. Sci.: Mater. Electron. 24, 2309 (2013)

34. L. Xu, F. Li, Y. Wang, J. Alloys Compnds. 501, 115 (2010)

35. N. Wu, T. C. Holgate, N. V. Nong, N. Pryds, S. Linderoth, J. Eur. Ceram. Soc. 34, 925 (2014)

36. Y. H. Lin, J. Lan, Z. J. Shen, Y. H. Liu, C. W. Nan, J. F. Li, Appl. Phys. Lett. 94, 072107 (2009)

Figure captions:

Figure 1. Powder X-ray diffraction patterns obtained for the $Ca_3Co_{4-x}Ti_xO_9$ samples; x = 0.00 (a); 0.01 (b); 0.03 (c); 0.05 (d); and 0.07 (e). The diffraction planes indicate the $Ca_3Co_4O_9$ phase and the * the $Ca_3Co_2O_6$ ones.

Figure 2. SEM micrographs performed on representative fractured sections of $Ca_3Co_{4-x}Ti_xO_y$ samples, for x = 0.00 (a); and 0.07 (b).

Figure 3. SEM micrograph performed on representative surface sections, corresponding to the $Ca_3Co_{4-x}Ti_xO_9$ samples for x = 0.00 (a); and 0.03 (b). Major grey contrast corresponds to the $Ca_3Co_{4-x}Ti_xO_9$ phase; the arrows indicate the $Ca_3Co_{2-x}Ti_xO_6$ phase which shows a similar contrast but different grain morphology.

Figure 4. Temperature dependence of the Seebeck coefficient, as a function of Ti content, in $Ca_3Co_{4-x}Ti_xO_9$ samples, for x = 0.00 (●); 0.01 (■); 0.03 (◆); 0.05 (▼); and 0.07 (▲).

Figure 5. Temperature dependence of the electrical resistivity, as a function of Ti content, in $Ca_3Co_{4-x}Ti_xO_9$ samples, for x = 0.00 (●); 0.01 (■); 0.03 (◆); 0.05 (▼); and 0.07 (▲).

Figure 6. Temperature dependence of the power factor, as a function of Ti content, in $Ca_3Co_{4-x}Ti_xO_9$ samples, for x = 0.00 (●); 0.01 (■); 0.03 (◆); 0.05 (▼); and 0.07 (▲).

Figure 1

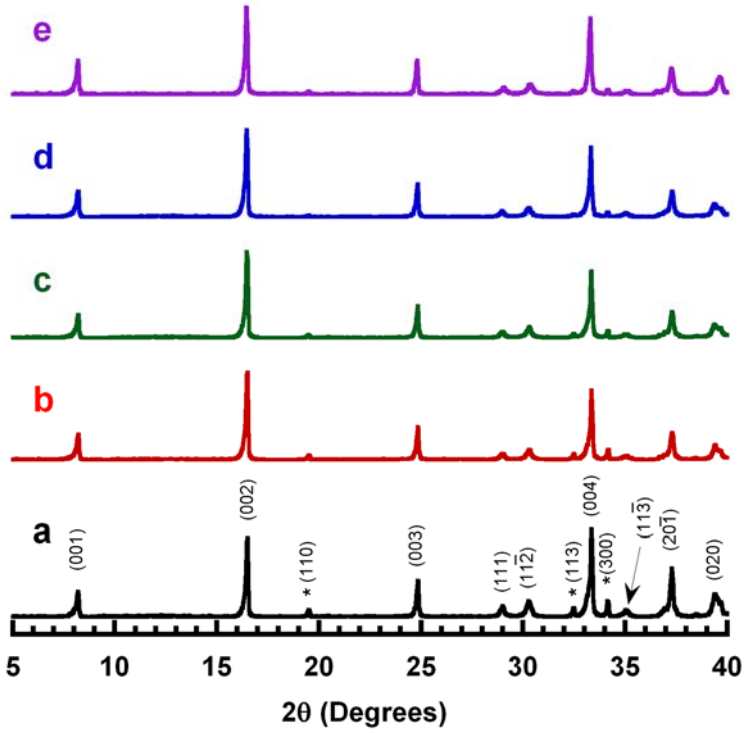
e
d
c
b
a
(001)
(002)
* (110)
(003)
(111)
(11$\bar{2}$)
* (113)
(004)
*(300)
(11$\bar{3}$)
(20$\bar{1}$)
(020)
5
10
15
20
25
30
35
40
2θ (Degrees)

Figure 2

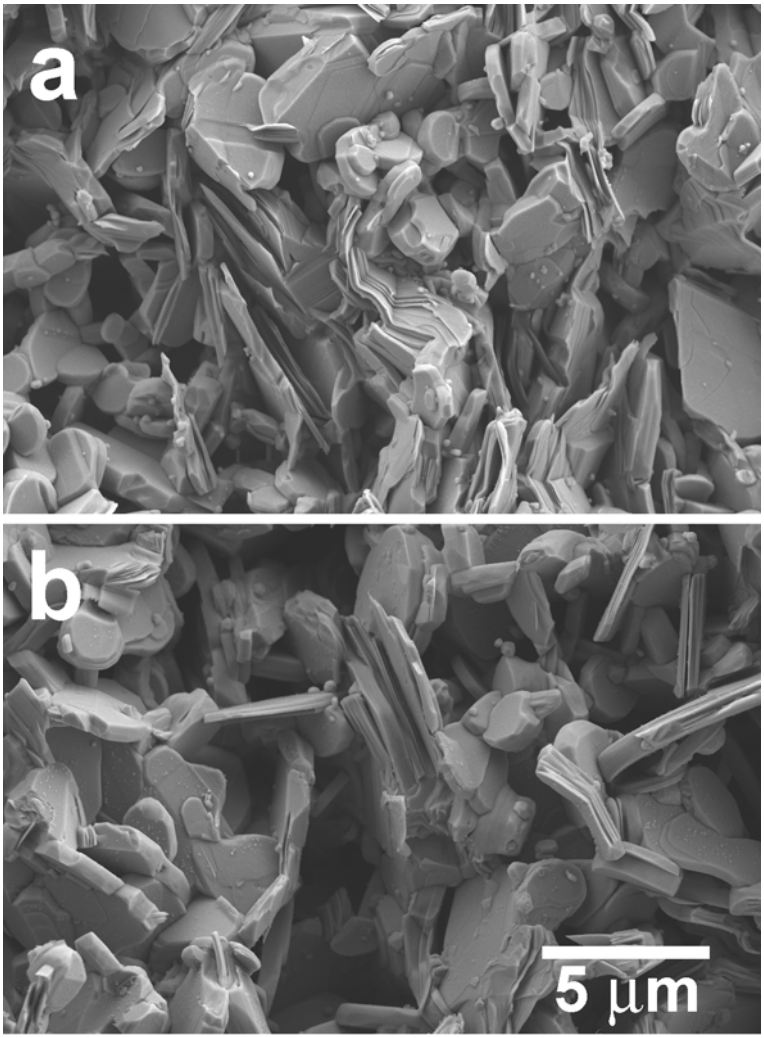

Figure 3

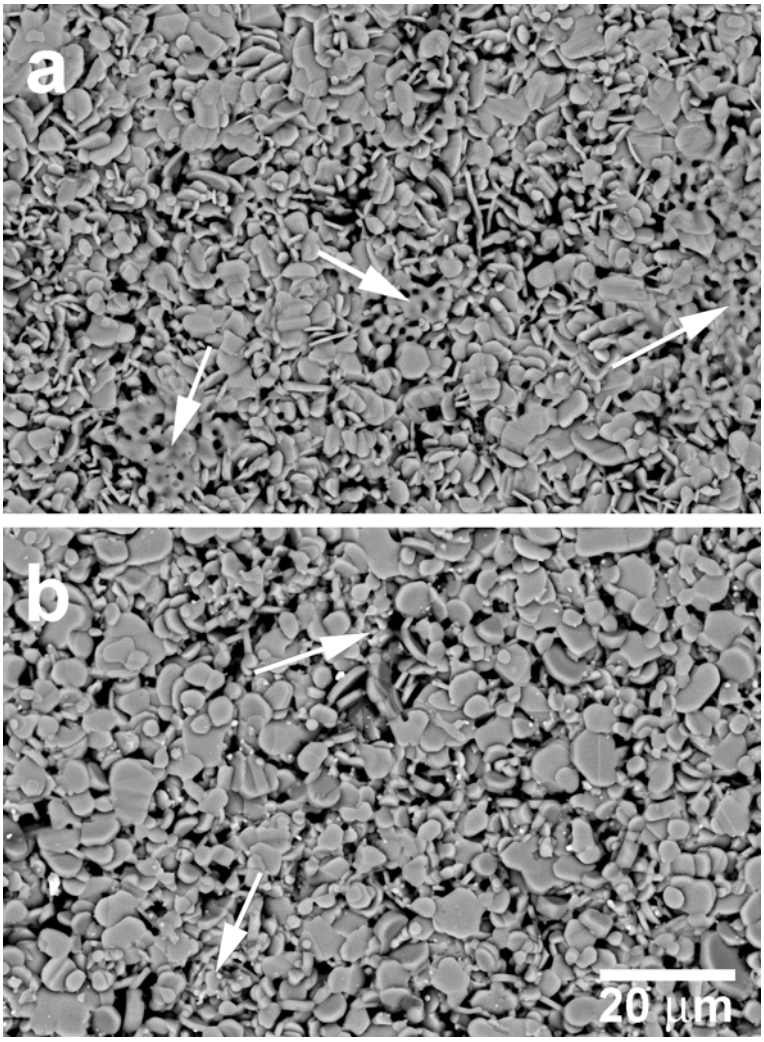

Figure 4

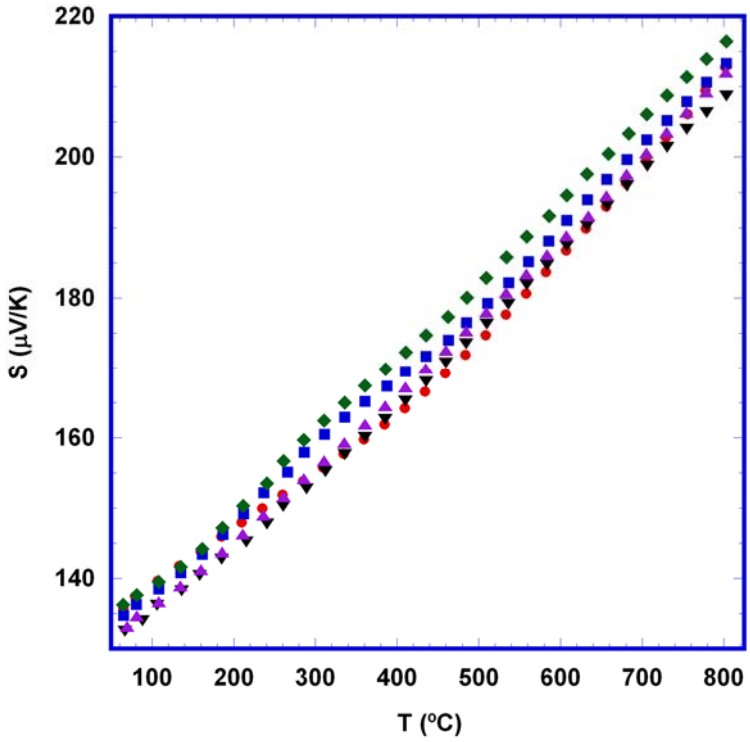

Figure 5

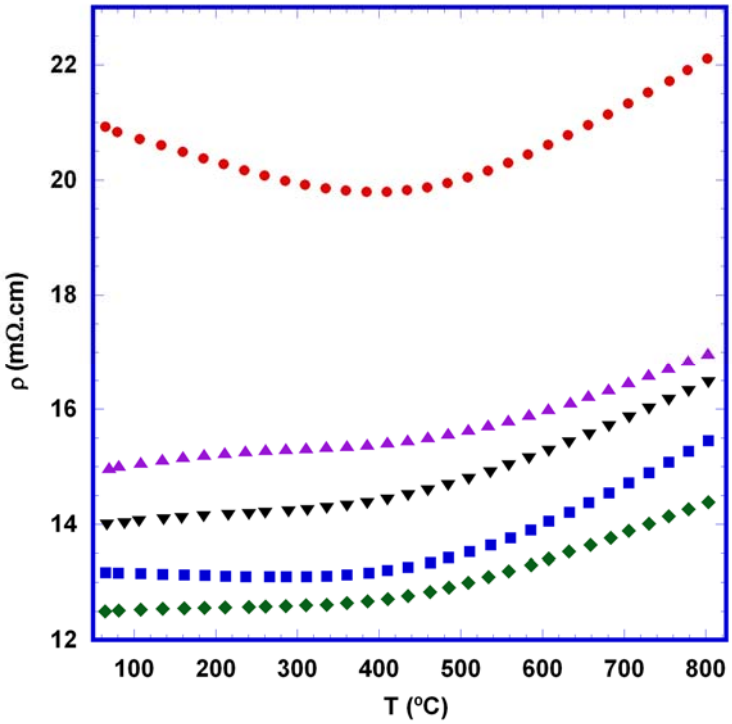

Figure 6

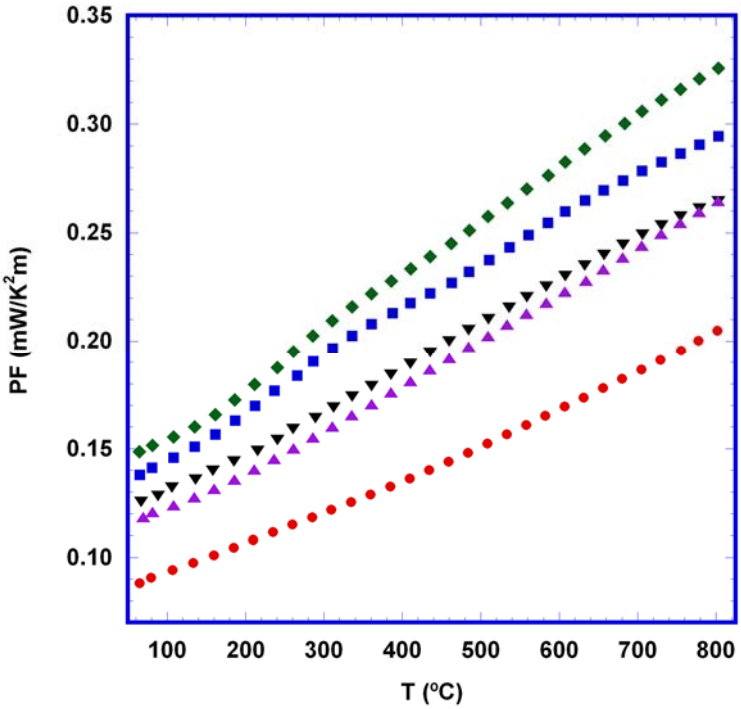
0.35
0.30
0.25
0.20
0.15
0.10
PF (mW/K²m)
100
200
300
400
500
600
700
800
T (ºC)